JOURNAL OF SYNCHROTRON RADIATION
ISSN 1600-5775

In situ X-ray absorption spectroscopic studies of photocatalytic oxidation of As(III) to less toxic As(V) by TiO_2 nanotubes

T.-L. Hsiung,[a] L.-W. Wei,[a] H.-L. Huang,[b] Y.-J. Tuan[a] and H. Paul Wang[a]*

[a]Department of Environmental Engineering, National Cheng Kung University, Tainan 70101, Taiwan, and [b]Department of Safety, Health and Environmental Engineering, National United University, Miaoli 36003, Taiwan. *Correspondence e-mail: wanghp@mail.ncku.edu.tw

Received 3 September 2020
Accepted 23 March 2021

Edited by R. W. Strange, University of Essex, United Kingdom

Keywords: arsenic; *in situ* XANES; TiO_2 nanotube; photocatalysis.

Arsenic in groundwater caused the black-foot disease (BFD) in many countries in the 1950–1960s. It is of great importance to develop a feasible method for removal of arsenic from contaminated groundwater in BFD endemic areas. Photocatalytic oxidation of As(III) to less toxic As(V) is, therefore, of significance for preventing any arsenic-related disease that may occur. By *in situ* synchrotron X-ray absorption spectroscopy, the formation of As(V) is related to the expense of As(III) disappearance during photocatalysis by TiO_2 nanotubes (TNTs). Under UV/Vis light irradiation, the apparent first-order rate constant for the photocatalytic oxidation of As(III) to As(V) is 0.0148 min^{-1}. It seems that As(III) can be oxidized with photo-excited holes while the not-recombined electrons may be scavenged with O_2 in the channels of the well defined TNTs (an opening of 7 nm in diameter). In the absence of O_2, on the contrary, As(III) can be reduced to As(0), to some extent. Cu(II) (CuO), as an electron acceptor, was impregnated on the TNTs surfaces in order to gain a better understanding of electron transfer during photocatalysis. It appears that As(III) can be oxidized to As(V) while Cu(II) is reduced to Cu(I) and Cu(0). The molecular-scale data are very useful in revealing the oxidation states and interconversions of arsenic during the photocatalytic reactions. This work has implications in that the toxicity of arsenic in contaminated groundwater or wastewater can be effectively decreased via solar-driven photocatalysis, which may facilitate further treatments by coagulation.

1. Introduction

Arsenic, which may cause brain, liver, lung, kidney, bladder and skin damage, has frequently been found in wastewater and groundwater in Bangladesh, India, Taiwan, Vietnam, Japan, Argentina, Mexico, Germany and USA (Singh *et al.*, 2015; Matta & Gjyli, 2016; Cicero *et al.*, 2017; Nazari *et al.*, 2017; Gomaa *et al.*, 2018). Arsenic-contaminated groundwater may be caused by natural weathering, dissolution of arsenic-bearing minerals as well as human activities such as burning of fossil fuels, mining, wood preservatives, pesticides and fertilizers. The maximum contaminant allowance of arsenic in drinking water was decreased from 50 to 10 μg L^{-1} by the US Environmental Protection Agency and the World Health Organization (Nazari *et al.*, 2017; Marinho *et al.*, 2019; Vera *et al.*, 2016). It is worth noting that As(III) has a greater toxicity (by 60 times approximately) and mobility than As(V) (Cicero *et al.*, 2017; Nazari *et al.*, 2017; Vera *et al.*, 2016; López-Muñoz *et al.*, 2017; Byrne *et al.*, 2018).

The common arsenic compounds that occur naturally are neutral H_3AsO_3 [As(III)] and $HAsO_4^{2-}$ [As(V)] when the

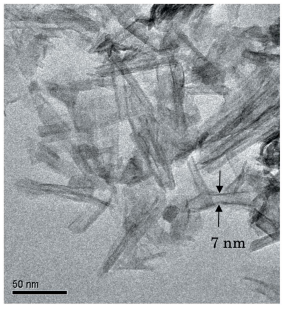

groundwater pH is less than 9.2 (Emmanuel *et al.*, 2019). Concentrations of arsenic (somewhat >500 p.p.m.) in wastewater could be decreased by coagulation with iron and aluminium salts; nevertheless, this has suffered from relatively low effectiveness and additional hazardous sludge to be treated (López-Muñoz *et al.*, 2017; Lata & Samadder, 2016). Pre-oxidation of As(III) to As(V) may facilitate the coagulation (Pires *et al.*, 2015). Chlorine, sodium hypochlorite, chlorine dioxide, ozone, hydrogen peroxide, permanganate (or manganese dioxide) and Fenton's reagents were frequently used in the oxidation of As(III) in wastewater (Ebrahiem *et al.*, 2017; Butnariu *et al.*, 2019). However, carcinogenic by-products such as halogenated hydrocarbons in those chemical oxidation processes may be formed (Lata & Samadder, 2016).

Molecular-scale data such as coordination number (CN), bond distance and oxidation state of select elements in a complicated matrix can be determined by X-ray absorption near-edge structure (XANES) and extended X-ray absorption fine-structure (EXAFS) spectroscopy (Kang & Wang, 2013; Huang *et al.*, 2003; Lin & Wang, 2000; Liu & Wang, 2004). By EXAFS, in the previous studies, we found that copper oxide clusters are involved in catalytic decomposition of NO and oxidization of chlorophenols (in supercritical water) (Huang *et al.*, 2003). These molecular-scale data turned out to be very useful in revealing the nature of the catalytic active species and reaction paths involved (Kang & Wang, 2013; Huang *et al.*, 2003; Lin & Wang, 2000; Liu & Wang, 2004). In separate experiments, by XANES, arsenic humic substance complexes were found to be associated with the black-foot disease that occurred in the seashore towns of Southwest Taiwan in the 1960s (Wang *et al.*, 2003). Studies on the photocatalytic oxidation of As(III) to less toxic As(V) are, therefore, of significance for preventing any arsenic-related disease that may occur.

TiO_2, possessing unique characteristics such as effective band-gap energy (3.0 eV) and high photo-stability, oxidation potential and availability, has been widely used in photocatalytic degradation of toxic organics, splitting of H_2O, and reduction of NO to N_2 (Meng *et al.*, 2015; Mikhaylov *et al.*, 2013; Ali & Metwally, 2014). Photocatalytic oxidation of As(III) effected by TiO_2, considered an environmentally friendly and economically attractive method, has gained great attention (Ryu & Choi, 2006; Yazdani *et al.*, 2017; Lescano *et al.*, 2014). However, a better understanding of the chemical structure of arsenic during photocatalytic oxidation is still lacking in the literature (Ryu & Choi, 2006). TiO_2 nanotubes (TNTs) containing a defined channel structure could be used for molecular-scale studies of arsenic during photocatalytic oxidation (Ge *et al.*, 2016; Crişan *et al.*, 2018; Nakata & Fujishima, 2012; Zhang *et al.*, 2015; Lijuan *et al.*, 2016). Thus the main objective of this work was to study the photocatalytic oxidation of As(III) effected by TNTs. Specifically, an *in situ* XANES spectroscopic cell that allows synchrotron X-ray as well as UV/Vis light irradiation simultaneously onto the TNTs during photocatalysis was used to reveal the photocatalytic reaction paths.

2. Materials and methods

The TNT photocatalysts were prepared by hydrothermal treatments of 12.5 g of nano TiO_2 (P25, Degussa) and 100 ml of NaOH (10 *M*, Merck) in a Teflon-lined autoclave at 380 K (under autogenous pressure) for three weeks to yield lamellar TiO_2 (Zhang *et al.*, 2015). The TNTs were obtained by scrolling the lamellar TiO_2 at a pH value of 7 (adjusted with a 0.2 N sulfuric acid solution) (Lijuan *et al.*, 2016). Copper [$Cu(NO_3)_2{\cdot}3H_2O$ (Fluka, 99%)] was impregnated on the TNT to yield a 5% CuO/TNT sample, which was dried at 333–345 K for 3 h and calcined at 573 K for 4 h before photocatalysis experiments.

Photocatalytic oxidation of As(III) ($NaAsO_2$) (Fluka) (10 m*M*) by the TNT was conducted with a home-made total reflectance photoreactor under UV/Vis light irradiation (250–800 nm) using a 300 W high-pressure Xe arc lamp (Newport, Model 6258). Images of the TNT photocatalyst were determined by high-resolution transmission electron microscopy (TEM) (JEM-3010, Jeol). Surface areas of the samples were measured on a Micromeritics analyzer (ASAP 2020).

The *in situ* Ti *K*-edge XANES and EXAFS spectra of arsenics compounds were determined on the wiggler beamline (17C) at the Taiwan National Synchrotron Radiation Research Center. Nano TiO_2 (P25), TNT and CuO/TNT (100 g L^{-1}) were used for photocatalytic oxidation under irradation [300 W high-pressure Xe arc lamp (Newport, Model 6258)]. A XANES spectroscopic cell that allows synchrotron X-ray and UV/Vis light simultaneously onto the photocatalysts during photocatalysis was employed (Hsiung *et al.*, 2006). A Si(111) double-crystal monochromator was used for selection of energy with an energy resolution ($\Delta E/E$) of 1.9×10^{-4}. Beam energy was calibrated by the adsorption edge of an arsenic powder at an energy of 11867 eV. All experimental data were collected in the fluorescence mode (Lytle detector). The absorption edge of arsenic in the TNT photocatalyst was determined at the half-height (precisely determined by the derivative) of the XANES spectrum after the pre-edge baseline subtraction and normalization to the maximum post-edge absorption. Semi-quantitative analyses of the edge spectra were conducted by the least-square fitting of the linear combination of standard spectra such as $NaAsO_2$ and Na_2HAsO_4 (Fluka). On average, an uncertainty limit of 5% corresponding to an error of ~2.0% in the fitting results was found. The isolated EXAFS data were normalized to the edge jump and converted to the wavenumber scale. Coordination numbers of arsenic were systematically varied in the course of the analysis within a given fitting range. Fitting model compounds was performed using *FEFFIT* from *UWXAFS 3.0* in combination with the multiple-scattering code *FEFF 8.0* simulation programs (Kang & Wang, 2013; Hsiung *et al.*, 2006).

3. Results and discussion

The TEM image of the TNT photocatalyst is shown in Fig. 1. It is clear that the TNTs have a one-dimensional multi-wall

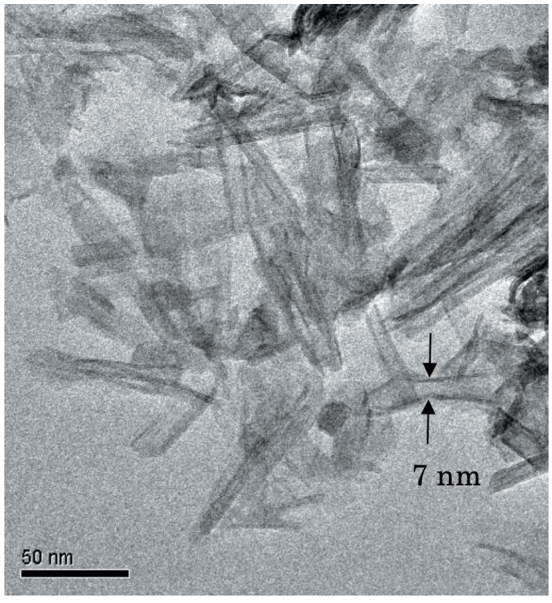

Figure 1
TEM image of the TNT photocatalyst.

tubular structure with a pore opening of about 7 nm and a length between 50 and 100 nm. In Fig. 2, a hysteresis loop at $P/P_0 > 0.60$ is found, which may be associated with the mesoporous structure in the TNT. The TNT has a higher surface area (286 $m^2\ g^{-1}$), which is mainly contributed by its mesopores, than the nano TiO_2 (47 $m^2\ g^{-1}$).

The *in situ* XANES spectra of arsenic during photocatalytic oxidation of As(III) by the TNT are shown in Fig. 3. The white-line absorptions of model compounds such as $NaAsO_2$ [As(III)] and Na_2HAsO_4 [As(V)] are observed at 11872 and 11876 eV, respectively. Under UV/Vis light irradiation for 210 min, the white-line absorption of arsenic is blue-shifted to 11876 eV, suggesting that the adsorbed As(III) on the TNT photocatalysts has been oxidized and forms As(V) (see Fig. 3). The component-fitted XANES spectra of arsenic under the UV/Vis light irradiation for 60 min (shown in the inset of Fig. 3) reveal oxidation (about 46%) of As(III) to As(V) on the TNT surface.

Table 1
Structure parameters of arsenic during photocatalytic oxidation of As(III) by the TNT.

R: bond distance; CN: coordination number; σ^2: Debye–Waller factor.

Reaction time (min)	Shell	*R* (Å)	CN	σ^2 (Å^2)
0	As—O	1.77	3.9	0.006
30	As—O	1.76	4.3	0.006
60	As—O	1.72	4.6	0.008
90	As—O	1.72	4.9	0.006
120	As—O	1.70	5.5	0.009
150	As—O	1.70	5.7	0.008
180	As—O	1.69	5.8	0.007
210	As—O	1.67	5.3	0.005
Model compounds				
$NaAsO_2$ [As(III)]	As—O	1.76	2.8	0.008
$AsHNa_2O_4$ [As(V)]	As—O	1.67	4.8	0.004

The EXAFS spectra of arsenic during photocatalytic oxidation effected by the TNT photocatalyst have also been recorded and analyzed in the *k* range 4.0–13.5 $Å^{-1}$. Their Debye–Waller factors (σ^2) are less than 0.01 $Å^2$ (see Table 1). The first-shell bond distances (As—O) of As(III) ($NaAsO_2$) and As(V) (Na_2HAsO_4) are 1.76 and 1.67 Å, respectively. Adsorption of As(III) on the TNT (without UV/Vis light irradiation) leads to an increase of averaged As—O bond distance (1.76 → 1.77 Å) and CN (2.8 → 3.9) if compared with the $NaAsO_2$ model compound. Moreover, a decrease of the averaged first-shell As—O bond distance (from 1.77 to 1.67 Å) and an increase of its CN (3.9 → 5.3) is also found during photocatalytic oxidation of As(III) on the TNT photocatalyst.

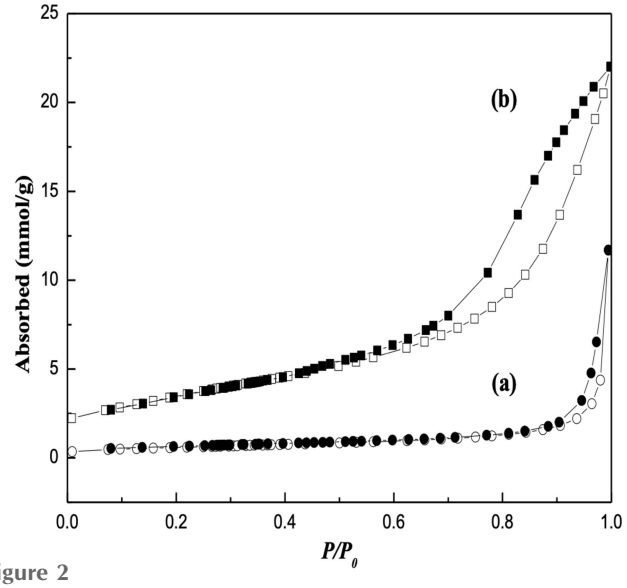

Figure 2
N_2 adsorption (filled symbols) and desorption (empty symbols) isotherms of (*a*) nano TiO_2 and (*b*) TNT.

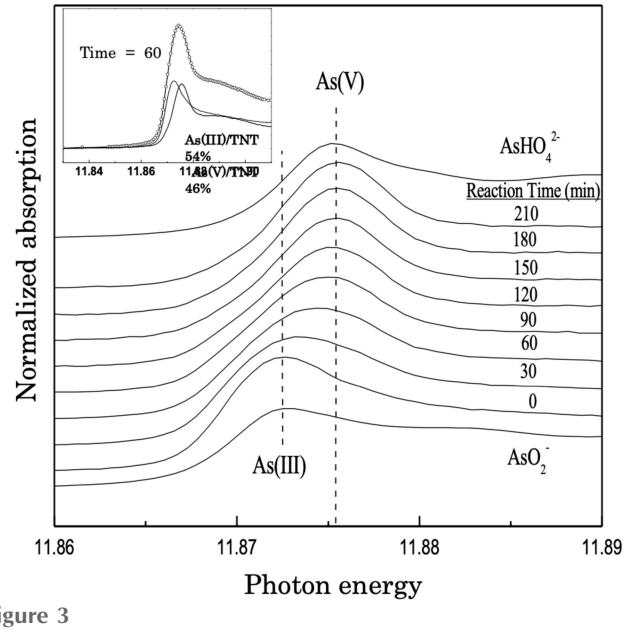

Figure 3
In situ XANES spectra of arsenic during photocatalytic oxidation of As(III) by TNT under UV/Vis light irradiation.

In Fig. 4, the interconversion of As(III) to As(V), as the formation of As(V) is at the expense of As(III) disappearance during photocatalysis, is observed. Complete oxidation of As(III) on the TNT photocatalysts is observed after 210 min of UV/Vis light irradiation. Note that on the nano TiO_2 (P25), the interconversion of As(III) to As(V) is not very effective, *i.e.* approximately 17% by the nano TiO_2 versus 90% by the TNT for 180 min irradiation (see Fig. 4). This has significant implications in that, in the well defined channels of the TNT, enhanced photocatalytic oxidation of As(III) may occur. Generally, hydroxyl radicals and superoxide radicals (yielded via photoexcited electron–hole pairs) may oxidize As(III) to form As(IV) species [such as $As^{IV}(OH)_4$, $As^{IV}O_3^-$, $HAs^{IV}O_3^-$ and $As^{IV}O_3^{2-}$] (López-Muñoz *et al.*, 2017). Nevertheless, the As(IV) intermediate species are not found by *in situ* XANES (see Fig. 4) in this study. Oxidation of As(III) to yield As(V) is the main photocatalytic reaction by the TNT in the presence of O_2 (in air). Dutta and co-workers found that photocatalytic oxidation of As(III) effected by nano TiO_2 following the zero-order kinetics (López-Muñoz *et al.*, 2017). In the present work, photocatalytic oxidation of As(III) on the nano TiO_2 also proceeds in the zero-order reaction kinetics. It seems that photocatalytic oxidation of As(III) to As(V) occurs mainly on the internal surfaces of the well defined mesopore in the TNT.

The photocatalytic interconversion of As(III) to As(V) on the CuO/TNT is also shown in Fig. 4. CuO could promote separation of electron–hole pairs and enhance photocatalytic oxidation of As(III) on nano TiO_2 (López-Muñoz *et al.*, 2017). In the present study, about 28% of As(V) is formed from photocatalytic oxidation of As(III) by the CuO/TNT for 210 min irradiation. It seems that the CuO [Cu(II)] may perturb oxidation between photocatalytically excited holes and adsorbed As(III) on TNT surfaces.

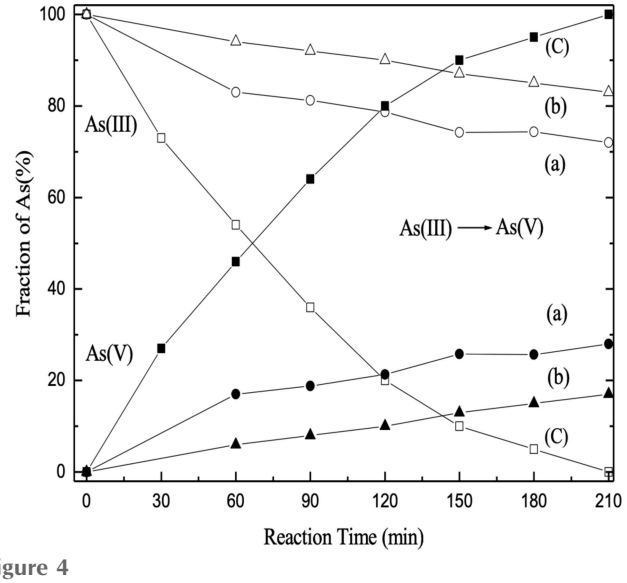

Figure 4
Photocatalytic oxidation of As(III) (empty symbols) to As(V) (filled symbols) effected by (*a*) nano TiO_2 (triangles), (*b*) Cu(II)/TNT (circles) and (*c*) TNT (squares) under UV/Vis light irradiation.

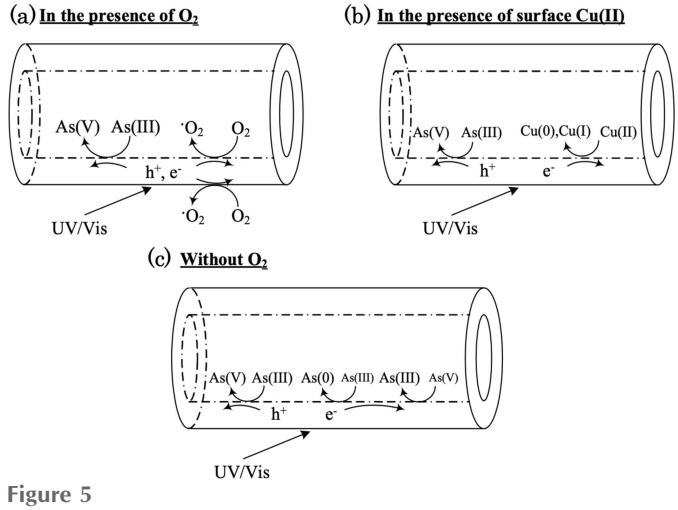

Figure 5
Schematic illustration of photocatalytic oxidation of As(III) effected by (*a*) TNT with O_2, (*b*) CuO/TNT with O_2 and (*c*) TNT without O_2.

The illustration for the photocatalytic oxidation of As(III) effected by the TNT is shown in Fig. 5. The *in situ* XANES spectra indicate that As(III) can be photocatalytically oxidized to mainly As(V) by the TNT in the presence of O_2 (in air) under UV/Vis light irradiation for 210 min. On the nano TiO_2, the zero-order reaction rate constant is 8.56 μM min^{-1}, while the apparent reaction rate constant (k) for the pseudo first-order interconversion of As(III) to As(V) [$\ln (C_0/C) = kt$] catalyzed by TNT is 0.0148 min^{-1}.

It is clear that, in the presence of O_2 (in air), As(V) is the exclusive species yielded from photocatalysis effected by TNT. It seems that dissolved oxygen acts as an electron scavenger [see Fig. 5(*a*)]. Note that, in Fig. 6, the XANES spectra between those for As(0) and As(III) are observed after photocatalysis effected by TNT for 210 min irradiation, suggesting that As(III) can be reduced to yield As(0), to some extent, in the absence of O_2.

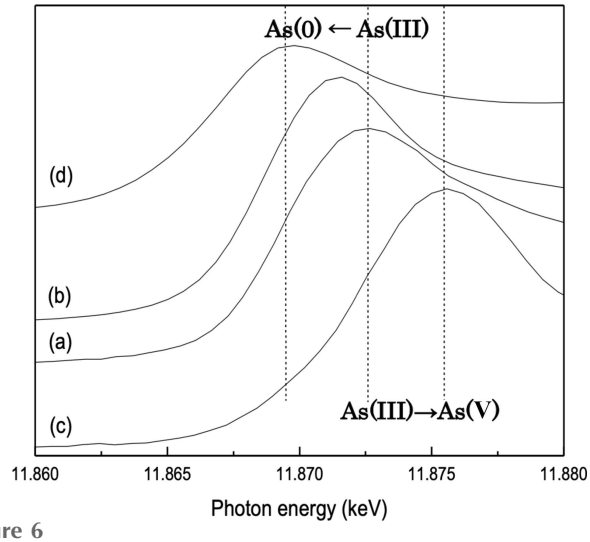

Figure 6
XANES spectra of arsenic (*a*) before and (*b*) after photocatalysis effected by TNT (*b*) without O_2 and (*c*) with O_2 (in air) for 210 min irradiation, and (*d*) As(0) (model compound).

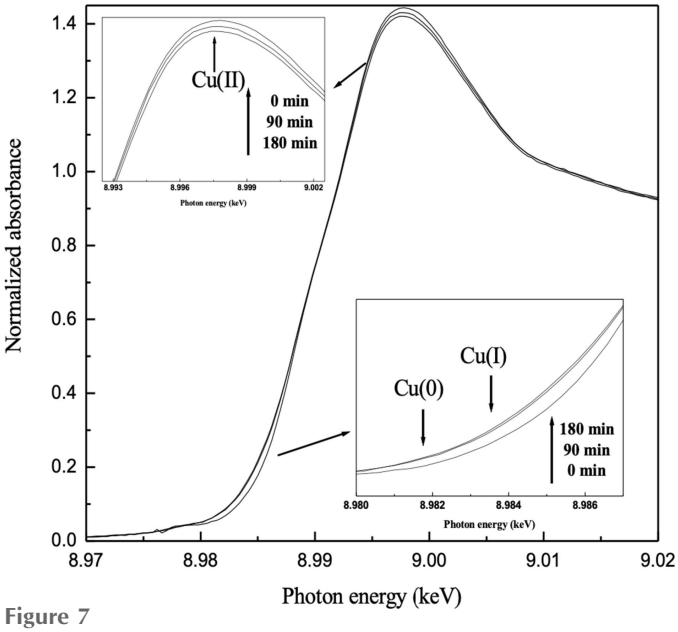

Figure 7
In situ XANES spectra of copper in the Cu(II)/TNT for photocatalytic oxidation of AS(III) under 90 min and 180 min irradiation.

Also, to enhance separation of photo-excited electron–hole pairs, photocatalytic oxidation of As(III) is carried out in the presence of 5% CuO/TNT [Fig. 5(*b*)]. CuO [Cu(II)] can also scavenge electrons. In Fig. 7, after photocatalysis effected by the CuO/TNT for 90 and 180 min irradiation, lower oxidation state copper [Cu(I) and Cu(0)] is found at the expense of the Cu(II) disappearance while As(III) is oxidized to As(V) on the TNT. Note that the intense band (white line) at 8994–9002 eV can be attributed to the 1*s*-to-4*p* transition, indicating the existence of the Cu(II) species, while Cu(0) and Cu(I) species are found at 8982 and 8982–8984 eV, respectively.

4. Conclusions

Observations by *in situ* XANES spectroscopy suggest that As(III) can be oxidized with photo-excited holes while the not-recombined electrons may be scavenged with O_2 on the surfaces of TNTs during photocatalysis. The apparent first-order rate constant for the photocatalytic inter-conversion of As(III) to As(V) is 0.0148 min^{-1}. Without O_2, As(III) can be reduced, to some extent. When Cu(II) (CuO) was dispersed on the TNT surfaces, an electron acceptor can cause As(III) to be oxidized to As(V) while low-oxidation state coppers [Cu(I) and Cu(0)] are formed. The molecular-scale data obtained using the *in situ* synchrotron X-ray absorption spectroscopy may implement a better and energy-efficient method for oxidation of arsenic by solar-driven photocatalysis to reduce toxicity, and may facilitate further treatment by coagulation.

Acknowledgements

The financial support of the Taiwan Ministry of Science and Technology, Bureau of Energy, and National Synchrotron Radiation Research Center (NSRRC) are gratefully. We also thank Y. W. Yang and Jyh-Fu Lee of the NSRRC for their assistance with the X-ray absorption experiments.

References

Ali, B. & Metwally, M. (2014). *Phys. Chem. Chem. Phys.* **16**, 7146–7160.
Butnariu, I. C., Stoian, O., Voicu, Ş., Iovu, H. & Paraschiv, G. (2019). *Ann. Fac. Eng. Hunedoara*, **17**, 175–179.
Byrne, C., Subramanian, G. & Pillai, S. C. (2018). *J. Environ. Chem. Eng.* **6**, 3531–3555.
Cicero, C. E., Mostile, G., Vasta, R., Rapisarda, V., Signorelli, S. S., Ferrante, M., Zappia, M. & Nicoletti, A. (2017). *Environ. Res.* **159**, 82–94.
Crişan, M., Mardare, D., Ianculescu, A., Drăgan, N., Niţoi, I., Crişan, D., Voicescu, M., Todan, L., Oancea, P., Adomniţei, C., Dobromir, M., Gabrovska, M. & Vasile, B. (2018). *Appl. Surf. Sci.* **455**, 201–215.
Ebrahiem, E. E., Al-Maghrabi, M. N. & Mobarki, A. R. (2017). *Arab. J. Chem.* **10**, S1674–S1679.
Emmanuel, B., Makhatha, E. & Nheta, W. (2019). *Energy Proc.* **157**, 966–971.
Ge, M., Cao, C., Li, S., Tang, Y., Wang, L., Qi, J., Huang, J., Zhang, K., Al-Deyab, S. S. & Lai, Y. (2016). *Nanoscale*, **8**, 5226–5234.
Gomaa, H., Shenashen, M. A., Yamaguchi, H., Alamoudi, A. S., Abdelmottaleb, M., Cheira, M. F. & El-Safty, S. A. (2018). *J. Cleaner Production*, **182**, 910–925.
Hsiung, T. L., Wang, H. P., Lu, Y. M. & Hsiao, M. C. (2006). *Radiat. Phys. Chem.* **75**, 2054–2057.
Huang, Y. J., Paul Wang, H. & Lee, J. F. (2003). *Appl. Catal. Environ.* **40**, 111–118.
Kang, H. Y. & Wang, H. P. (2013). *Environ. Sci. Technol.* **47**, 7380–7387.
Lata, S. & Samadder, S. R. (2016). *J. Environ. Manage.* **166**, 387–406.
Lescano, M., Zalazar, C. & Brandi, R. (2014). *Environ. Sci. Pollut. Res.* **22**, 3865–3875.
Lijuan, H., Zheng, M., Zhihe, L., Gang, L., Jiantai, M. & Xingcai, A. (2016). *RSC Adv.* **6**, 6643–6650.
Lin, K. S. & Wang, H. P. (2000). *Langmuir*, **16**, 2627–2631.
Liu, S. H. & Wang, H. P. (2004). *J. Environ. Qual.* **33**, 1280–1287.
López-Muñoz, M. J., Arencibia, A., Segura, Y. & Raez, J. M. (2017). *Catal. Today*, **280**, 149–154.
Marinho, B. A., Cristóvão, R. O., Boaventura, R. A. R. & Vilar, V. J. P. (2019). *Environ. Sci. Pollut. Res.* **26**, 2203–2227.
Matta, G. & Gjyli, L. (2016). *J. Chem. Pharm. Sci.* **9**, 718–725.
Meng, J. P., Shang, C. L., Yu, C. L. & Chang, C. H. (2015). *J. Hazard. Mater.* **288**, 168–175.
Mikhaylov, R. V., Lisachenko, A. A., Shelimov, B. N., Kazansky, V. B., Martra, G. & Coluccia, S. (2013). *J. Phys. Chem. C*, **117**, 10345–10352.
Nakata, K. & Fujishima, A. (2012). *J. Photochem. Photobiol. Photochem. Rev.* **13**, 169–189.
Nazari, A. M., Radzinski, R. & Ghahreman, A. (2017). *Hydrometallurgy*, **174**, 258–281.
Pires, V. G. R., Lima, D. R. S., Aquino, S. F. D. & Libânio, M. (2015). *Braz. J. Chem. Eng.* **32**, 409–419.
Ryu, J. & Choi, W. (2006). *Environ. Sci. Technol.* **40**, 7034–7039.
Singh, R., Singh, S., Parihar, P., Singh, V. P. & Prasad, S. M. (2015). *Ecotoxicol. Environ. Saf.* **112**, 247–270.
Vera, R., Fontàs, C. & Anticó, E. (2016). *Environ. Sci. Pollut. Res.* **24**, 10939–10948.
Wang, H. C., Wang, H. P., Peng, C. Y., Liu, H. L. & Huang, H. L. (2003). *Bull. Environ. Contam. Toxicol.* **71**, 798–803.
Yazdani, M., Bhatnagar, A. & Vahala, R. (2017). *Chem. Eng. J.* **316**, 370–382.
Zhang, Y., Jiang, Z., Huang, H., Lim, L. Y., Li, W., Deng, J., Gong, D., Tang, Y., Lai, Y. & Chen, Z. (2015). *J. R. Soc. Chem.* **5**, 79479–79510.